THERMOMECHANICALLY INDUCED PRE AND POSTBUCKLING OF GENERAL STRUCTURE

Joseph Padovan
The University of Akron
Akron, Ohio 44325

This paper develops an algorithmic solution strategy which enables handling the positive/indefinite stiffness characteristics associated with the pre and postbuckling of structures subject to complex thermomechanical loading fields. The flexibility of the procedure is such that it can be applied to both finite difference and element type simulations. Due to the generality of the algorithmic approach developed, both kinematic and thermal/mechanical type material nonlinearity including inelastic effects can be treated. This includes the possibility of handling completely general thermomechanical boundary conditions. To demonstrate the scheme, the results of several benchmark problems is presented.

INTRODUCTION

Literally a multitude of studies have been reported on the isothermal simulation of problems wherein kinematic and/or material nonlinearity is excited. In recent years, most typically such work involved the use of the powerful finite element (FE) scheme [1]. In contrast, much less work is available for nonisothermal versions of such problems. This is an outgrowth of several main factors namely:

i) Unlike mechanical type loads which are generally applied at specific points around a given structure, transient thermally induced loads occur at every body point causing complex distributed loading and unloading fields which typically induce difficulties in simulating proper inelastic type behavior;

ii) Since thermal loads are internally induced, for nonlinear situations, it is typically quite difficult to adequately forecast the level of incrementation necessary for nonlinear equation solvers to yield converged solutions without involving an expensive time consuming trial and error procedure;

iii) For problems with highly nonlinear kinematic behavior, little is understood of the process of thermomechanical interaction; and lastly,

iv) Thermomechanically induced pre and postbuckling behavior exhibits indefinite stiffness characteristics [2]; such behavior precludes the use of the classical form of the incremental Newton Raphson (INR) scheme which is restricted to problems with a given definiteness [2,3].

Since numerous thermomechanical problems fall into the foregoing categories, this paper will consider the development of a solution strategy which

bypasses the difficulties denoted by items i) - iv) noted earlier. Specifically, a constrained type strategy [4-7] will be developed for use with either the finite element [1] or difference methodologies. The generality of the procedure is such that both pre and postbuckling behavior can be handled along with arbitrary kinematic and material nonlinearity. In this context, problems exhibiting indefinite stiffness characteristics can be handled.

GOVERNING EQUATIONS: MECHANICAL

Assuming the possibility of large deformations, the equations of motion complementing the thermal formulation are given by the expression

$$\frac{\partial}{\partial a_j}\left(S_{jk}\left(\delta_{ik} + \frac{\partial u_i}{\partial a_k}\right)\right) + g_{oi} = \rho_o \frac{\partial^2 u_i}{\partial t} \tag{2.1}$$

where g_{oi} designates the body force vector, δ_{ik} is the Kronecker delta, S_{ji} the second Piola Kirchhoff stress tensor, u_i the deflection vector and a_j the Lagrangian coordinates. For the current purposes, the Lagrangian strain measure L_{ij} is employed in conjunction with S_{ij} namely

$$L_{ij} = \frac{1}{2}\left(\frac{\partial u_i}{\partial a_j} + \frac{\partial u_j}{\partial a_i} + \frac{\partial u_\ell}{\partial a_i}\frac{\partial u_\ell}{\partial a_j}\right. \tag{2.2}$$

In terms of the S_{ij} and L_{ij} measures, the thermoelastic-plastic behavior is handled in terms of the usual yield surface flow rule assumption. The creep effects will be treated in terms of strain hardening concepts wherein variations in creep rate depend on the existing strain rate. From a computational point of view, the overall thermoelastic-plastic-creep behavior is solved via incremental type flow rules. Under the condition of large deformation moderate strain behavior and the usual flow rule assumption, the following incremental type constitutive relation is adopted, that is [8]

$$\Delta \underset{\sim}{S} = [D_{ep}](\Delta \underset{\sim}{L} - \Delta \underset{\sim}{L}_C - \Delta \underset{\sim}{L}_T) \tag{2.3}$$

where $[D_{ep}]$ is the elastic-plastic material stiffness and $\Delta \underset{\sim}{L}$, $\Delta \underset{\sim}{L}_C$ and $\Delta \underset{\sim}{L}_T$ are increments in Lagrangian creep and thermal strain. For the current work, $\Delta \underset{\sim}{L}_C$ is expressed in terms of mechanical equations of state. In particular, it takes the form

$$\Delta \underset{\sim}{L}_C = \Delta t\, \gamma\, \underset{\sim}{S}_d \tag{2.4}$$

where S_d is the deviatoric stress and

$$\gamma = \frac{1}{\sigma_d}\frac{\partial \varepsilon_c}{\partial t} \tag{2.5}$$

such that σ_d and $\frac{\partial \varepsilon_c}{\partial t}$ are respectively the equivalent stress and creep strain rates. Lastly, the increment in thermal strain appearing in (2.3) is defined by

$$\Delta \underset{\sim}{L}_T = \underset{\sim}{\alpha} \Delta T \tag{2.6}$$

where $\underset{\sim}{\alpha}$ is the thermal expansion coefficient matrix and ΔT is the temperature increment. Note, based on the thermal fields generated earlier, it follows that the various coefficients are temperature dependent.

In the context of (2.3) it follows that depending on the load step, the current stress state is given by the expression

$$\underset{\sim}{S} = \Sigma \Delta \underset{\sim}{S} \tag{2.7}$$

where the matrix S takes the form

$$\underset{\sim}{S}' = (\underset{\sim}{S}_{11}, \underset{\sim}{S}_{22}, \underset{\sim}{S}_{33}, \underset{\sim}{S}_{12}, \underset{\sim}{S}_{23}, \underset{\sim}{S}_{31}) \tag{2.8}$$

Noting the linear structure of $\Delta \underset{\sim}{S}$, we see that the incremental scheme enables the following segregation of contributing components namely

$$\underset{\sim}{S} = \underset{\sim}{S}_{ep} + \underset{\sim}{S}_{epc} + \underset{\sim}{S}_{epT} \tag{2.9}$$

where

$$\underset{\sim}{S}_{ep} = \Sigma \Delta \underset{\sim}{S}_{ep} \tag{2.10}$$

$$\underset{\sim}{S}_{epc} = \Sigma \Delta \underset{\sim}{S}_{epc} \tag{2.11}$$

$$\underset{\sim}{S}_{epT} = \Sigma \Delta \underset{\sim}{S}_{epT} \tag{2.12}$$

such that

$$\Delta \underset{\sim}{S}_{ep} = [D_{ep}] \, \Delta \underset{\sim}{L} \tag{2.13}$$

$$\Delta \underset{\sim}{S}_{epc} = - [D_{ep}] \, \Delta \underset{\sim}{L}_C \tag{2.14}$$

$$\Delta \underset{\sim}{S}_{epT} = - [D_{ep}] \, \Delta \underset{\sim}{L}_T \tag{2.15}$$

As will be seen later, such a partitioning of the stress state will enable the establishment of an improved control of successive iterates during the incrementation process.

FE FORMULATION/SOLUTION ALGORITHM: MECHANICAL

Following the thermal formulation, we shall employ a displacement type procedure to develop the requisite mechanical FE expressions. In this context, the deflection field is approximated by

$$\underset{\sim}{U} = [N_U] \underset{\sim}{Y} \tag{3.1}$$

where

$$\underset{\sim}{U}' = (u_1, u_2, u_3) \tag{3.2}$$

such that $[N_U]$ is the displacement type shape function while Y is the nodal deflection vector. For consistencies sake, the same order polynomial is used for both the thermal and mechanical phases. Based on (3.1) and the virtual work principle, the following FE expression can be developed [1]

$$[M_U]\ddot{\underset{\sim}{Y}} + \int_{V_o} [B_U^*]' \underset{\sim}{S}\, dv = \underset{\sim}{F}_{ext} \tag{3.3}$$

where

$$[B_U^*] = [B_U] + [B_n][G] \tag{3.4}$$

$$[M_U] = \int_{V_o} \rho_o\, [N_U]'[N_U]\, dv \tag{3.5}$$

$$\underset{\sim}{F}_{ext} = \underset{\sim}{F}_{nodal} + \int_{V_o} [N_U]'\, \underset{\sim}{g}_{ext}\, dv \tag{3.6}$$

such that

$$\underset{\sim}{g}_{ext} = (g_1, g_2, g_3) \tag{3.7}$$

Note $\underset{\sim}{F}_{nodal}$ represents the externally applied nodal loads.

Since dynamic postbuckling problems will be the subject of another paper, for the current purposes, we shall consider quasi-static thermo-mechanical problems. In this context, (3.3) reduces to the form

$$\int_{V_o} [B_U^*]'\, \underset{\sim}{S}\, dv = \underset{\sim}{F}_{ext} \tag{3.8}$$

To simplify the development of the requisite solution algorithm, the partitioned form of $\underset{\sim}{S}$ will be used to recast (3.8) into a more tractable form. Before doing so, we note that due to their analytical form, the creep and thermal partitions of $\underset{\sim}{S}$ can be lumped with $\underset{\sim}{F}_{ext}$ to yield a pseudo applied force field namely

$$\underset{\sim}{F} = \underset{\sim}{F}_{ext} - \int_{V_o} [B_U^*]' (\underset{\sim}{S}_{epc} + \underset{\sim}{S}_{epT})\, dv \tag{3.9}$$

Hence (3.8) reduces to the form

$$\underset{\sim}{F} = \int_{V_o} [B_U^*]'\, \underset{\sim}{S}_{ep}\, dv \tag{3.10}$$

Since $\underset{\sim}{S}_{epc}$ and $\underset{\sim}{S}_{epT}$ are time dependent terms, the solution to (3.10) requires the introduction of a time stepping algorithm to generate the requisite solution. This is achieved by expanding (3.10) in truncated Taylor series. To start, $\underset{\sim}{Y}(t+\Delta t)$ is expanded to yield

$$\underset{\sim}{Y}(t+\Delta t) = \underset{\sim}{Y}(t) + \Delta\underset{\sim}{Y} \tag{3.11}$$

Substituting (3.11) into (3.10) and truncating higher order terms yields the expression

$$\int_{V_o} [B_U^*]' \, \underset{\sim}{S}_{ep} \, dv \Big|_{t+\Delta t} = \int_{V_o} [B_U^*]' \, \underset{\sim}{S}_{ep} \, dv \Big|_{t} + [K_U] \Big|_{t} \, \underset{\sim}{\Delta Y} \tag{3.12}$$

where

$$[K_U] \Big|_{t} = \int_{V_o} ([G]'[S][G] + [B_U^*]'[D_{ep}][B_U^*]) \Big|_{t} \, dv \tag{3.13}$$

such that [S(t)] is the prestress matrix at time t. Based on the definition of pseudo force, Eq. (3.9), it follows that

$$\underset{\sim}{F} \Big|_{t+\Delta t} = \underset{\sim}{F}_{ext} \Big|_{t+\Delta t} - \int_{V_o} [B_U^*]' \Big|_{t} \, (\underset{\sim}{S}_{epC} + \underset{\sim}{S}_{epT}) \Big|_{t+\Delta t} \, dv \tag{3.14}$$

Now in terms of (3.10), (3.12) and (3.14), we obtain the following time stepping Newton Raphson type algorithm, that is

$$\underset{\sim}{F}_{ext} \Big|_{t+\Delta t} - \int_{V_o} [B_U^*]' \Big|_{t} \, (\underset{\sim}{S}_{epC} + \underset{\sim}{S}_{epT}) \Big|_{t+\Delta t} \, dv =$$

$$\int_{V_o} [B_U^*]' \, \underset{\sim}{S}_{ep} \Big|_{t} \, dv + [K_U] \Big|_{t} \, \underset{\sim}{\Delta Y} \tag{3.15}$$

Based on the use of such a relation, successive time steps lead to the following thermomechanical history namely

t	T(t)	$\underset{\sim}{S}$(t)	$\underset{\sim}{L}$(t)	...
0	T(0)	$\underset{\sim}{S}$(0)	$\underset{\sim}{L}$(0)	...
Δt	T(Δt)	$\underset{\sim}{S}$(Δt)	$\underset{\sim}{L}$(Δt)	...
$2\Delta t$	T($2\Delta t$)	$\underset{\sim}{S}$($2\Delta t$)	$\underset{\sim}{L}$($2\Delta t$)	...
$3\Delta t$	T($3\Delta t$)	$\underset{\sim}{S}$($3\Delta t$)	$\underset{\sim}{L}$($3\Delta t$)	...
$4\Delta t$	T($4\Delta t$)	$\underset{\sim}{S}$($4\Delta t$)	$\underset{\sim}{L}$($4\Delta t$)	...
⋮	⋮	⋮	⋮	
$i\Delta t$	T($i\Delta t$)	$\underset{\sim}{S}$($i\Delta t$)	$\underset{\sim}{L}$($i\Delta t$)	...

As noted earlier, the NR base of (3.15) suffers from several shortcomings. The more important of these are:

1. Cannot handle turning points (buckling);
2. No direct control on successive iterations; and,
3. Difficult to ascertain zones of convergence as solution proceeds.

Such drawbacks will be circumvented through the use of constraints in the manner of Padovan and Arechaga [6]. Specifically the load increments

associated with successive time steps will be constrained. Such a process leads to nonuniform time stepping. From the nature of (3.15) it follows that constraints must be imposed on increments in the pseudo load F. For the current purposes the hyper-elliptic constraint surface (HECS) of Padovan, Tovichakchaikul and Arechaga [7] will be employed to control successive iterations of a given time step. Such a process is illustrated in Fig. 1. The development of the requisite constraint algorithm for the given problem requires several main steps, namely:

i) Establish form of INR extrapolation for a given iteration;
ii) Establish shape and size of HECS;
iii) Determine intersection of HECS and INR extrapolation;
iv) Establish iterative/time stepping aspects of solution algorithm; and,
v) Establish information required for next time step.

To start the development, it follows from Fig. 1 that the hyperline defining the INR extrapolation takes the form

$$[K_{UB}](\underset{\sim}{y}-\underset{\sim}{y}_B) = (\underset{\sim}{f}-\underset{\sim}{f}_B) \tag{3.16}$$

On solving for y we obtain

$$\underset{\sim}{y} = \underset{\sim}{y}_B + [K_{UB}]^{-1}(\underset{\sim}{f}-\underset{\sim}{f}_B) \tag{3.17}$$

such that

$$\underset{\sim}{f}_B = \underset{\sim}{F}_B - \underset{\sim}{F}_A \tag{3.18}$$

$$\underset{\sim}{y}_B = \underset{\sim}{Y}_B - \underset{\sim}{Y}_A \tag{3.19}$$

The HECS appearing in Fig. 1 is given by the following normed polynomial expression

$$||\underset{\sim}{f}||^2 + \mu_A||\underset{\sim}{y}||^2 = ||\underset{\sim}{f}_C||^2 \tag{3.20}$$

such that

$$\underset{\sim}{f}_C = \underset{\sim}{F}_C - \underset{\sim}{F}_A \tag{3.21}$$

The parameter μ_A appearing in (3.21) regulates the aspect ratio (abscissa/ordinate) of the HECS.

The intersection of the HECS and INR extrapolation occurs at point I as defined in Fig. 1. Specifically the coordinates of position I are given by

$$\underset{\sim}{y}_I = \underset{\sim}{Y}_I - \underset{\sim}{Y}_A \tag{3.22}$$

$$\underset{\sim}{f}_I = \lambda^I (\underset{\sim}{F}_C - \underset{\sim}{F}_A) \tag{3.23}$$

such that λ^I is a single parameter constraint on the allowable load step size and hence the interval in time utilized. Based on (3.22) and (3.23),

it follows that (3.17) and (3.20) yield the expressions

$$\underset{\sim}{y}_I = \underset{\sim}{y}_B + [K_{UB}]^{-1}(\underset{\sim}{f}_I - \underset{\sim}{f}_B) = \underset{\sim}{y}_B + [K_{UB}]^{-1}(\lambda^I \underset{\sim}{f}_C - \underset{\sim}{f}_B) \tag{3.24}$$

$$||\underset{\sim}{f}_I||^2 + \mu_A||\underset{\sim}{y}_I||^2 = ||\underset{\sim}{f}_C||^2 \tag{3.25}$$

In terms of (3.24), (3.25) takes the form

$$||\lambda^I \underset{\sim}{f}_C||^2 + \mu_A||\underset{\sim}{y}_B + [K_{UB}]^{-1}(\lambda^I \underset{\sim}{f}_C - \underset{\sim}{f}_B)||^2 = ||\underset{\sim}{f}_C||^2 \tag{3.26}$$

Expanding (3.26) and collecting like terms in λ^I yields the following polynomial identity namely

$$(\lambda^I)^2\alpha_{1I} + 2\lambda^I\alpha_{2I} + \alpha_{3I} = 0 \tag{3.27}$$

where

$$\alpha_{1I} = ||\underset{\sim}{F}_C||^2 + \mu_A||[K_{UB}]^{-1}\underset{\sim}{F}_C||^2 \tag{3.28}$$

$$\alpha_{2I} = \mu_A(\underset{\sim}{y}_B)'[K_{UB}]'\underset{\sim}{f}_B \tag{3.29}$$

$$\alpha_{3I} = ||\underset{\sim}{y}_B - [K_{UB}]^{-1}\underset{\sim}{f}_B||^2 - ||\underset{\sim}{f}_C||^2 \tag{3.30}$$

Solving (3.27) for λ^I, we obtain

$$\lambda^I = \frac{1}{\alpha_{1I}}\{-\alpha_{2I} \pm \sqrt{(\alpha_{2I})^2 - \alpha_{1I}\alpha_{3I}}\} \tag{3.31}$$

Based on (3.22), (3.24) and (3.31), $\underset{\sim}{Y}_I$ the nodal deflection associated with the I^{th} intersection of the INR extrapolation and the HECS takes the form

$$\underset{\sim}{Y}_I = \underset{\sim}{Y}_A + \underset{\sim}{y}_B + [K_{UB}]^{-1}\{\frac{1}{\alpha_{1I}}(-\alpha_{2I} \pm \sqrt{(\alpha_{2I})^2 - \alpha_{1I}\alpha_{3I}})\ \underset{\sim}{f}_C - \underset{\sim}{f}_B\} \tag{3.32}$$

To establish the requisite time stepping aspects of the solution algorithm, the following variables must be redefined in terms of incrementation namely $\underset{\sim}{Y}_A$, $\underset{\sim}{Y}_B$, $\underset{\sim}{Y}_I - \underset{\sim}{y}_B$, $\underset{\sim}{F}_A$, $\underset{\sim}{F}_B$, $\underset{\sim}{F}_C$ and $[K_{UB}]$. Letting ℓ denote the time step number and i the iteration count, it follows that positions A, B and I in Fig. 1 designate the location of the 0^{th}, i^{th} and $(i+1)^{th}$ iterations. In this context, it follows that

$$\underset{\sim}{Y}_A = \underset{\sim}{Y}^0_{\ell+1} \tag{3.33}$$

$$\underset{\sim}{Y}_B = \underset{\sim}{Y}^i_{\ell+1} = \underset{\sim}{Y}^0_{\ell+1} + \sum_{k=1}^{i} \Delta\underset{\sim}{Y}^i_{\ell+1} \tag{3.34}$$

$$\underset{\sim}{y}_I - \underset{\sim}{y}_B = \Delta\underset{\sim}{Y}^{i+1}_{\ell+1} \tag{3.35}$$

The time associated with point A is the summation of the ℓ preceeding constrained time steps. Hence, since the interval utilized over a given load step is $\lambda_k^{\nabla}\Delta t$, it follows that the time at the end of the ℓ^{th} step is given by

$$t_\ell^\lambda = \sum_{k=1}^{\ell} \lambda_k^{\nabla}\Delta t \tag{3.36}$$

such that λ_k^{∇} is the finally converged value of the constraint for the k^{th} step.

Employing the foregoing nomenclature, it follows that

$$\underset{\sim}{F}_A = \int_{V_o} [B_U^*(\underset{\sim}{Y}^o_{\ell+1})]^T \underset{\sim}{S}_{ep}(\underset{\sim}{Y}^o_{\ell+1})\, dv \tag{3.37}$$

$$\underset{\sim}{F}_B = \int_{V_o} [B_U^*(\underset{\sim}{Y}^i_{\ell+1})]^T \underset{\sim}{S}_{ep}(\underset{\sim}{Y}^i_{\ell+1})\, dv \tag{3.38}$$

$$\underset{\sim}{F}_C = \underset{\sim}{f}_{ext}\Big|_{t_\ell^\lambda+\Delta t_{\ell+1}} - \int_{V_o} [B_U^*(\underset{\sim}{Y}^i_{\ell+1})]\,(\underset{\sim}{S}^i_{epC} + \underset{\sim}{S}^i_{epT})\Big|_{t_\ell^\lambda+\Delta t_{\ell+1}} dv \tag{3.39}$$

The various stress components appearing in (3.37) - (3.39) take the form

$$\underset{\sim}{S}_{ep}(\underset{\sim}{Y}^o_{\ell+1}) = \sum_{k=1}^{\ell} \Delta\underset{\sim}{S}_{ep}(\underset{\sim}{Y}^o_k) \tag{3.40}$$

$$\underset{\sim}{S}_{ep}(\underset{\sim}{Y}^i_{\ell+1}) = \underset{\sim}{S}_{ep}(\underset{\sim}{Y}^o_{\ell+1}) + \Delta\underset{\sim}{S}_{ep}(\underset{\sim}{Y}^i_{\ell+1}) \tag{3.41}$$

$$\underset{\sim}{S}_{epC}(t_\ell^\lambda) = \sum_{k=1}^{\ell} \Delta\underset{\sim}{S}_{ep_C}(t_{k-1}^\lambda + \lambda_k^{\nabla}\Delta t_k) \tag{3.42}$$

$$\underset{\sim}{S}^i_{epC}(t_\ell^\lambda + \Delta t) = \underset{\sim}{S}_{epC}(t_\ell^\lambda) + \Delta\underset{\sim}{S}^i_{epC}(t_\ell^\lambda+\Delta t) \tag{3.43}$$

$$\underset{\sim}{S}_{epT}(t_\ell^\lambda) = \sum_{k=1}^{\ell} \Delta\underset{\sim}{S}_{epT}(t_{k-1}^\lambda+\lambda_k^{\nabla}\Delta t_k) \tag{3.44}$$

$$\underset{\sim}{S}^i_{epT}(t_\ell^\lambda+\Delta t) = \underset{\sim}{S}_{epT}(t_\ell^\lambda) + \Delta\underset{\sim}{S}^i_{epT}(t_\ell^\lambda+\Delta t) \tag{3.45}$$

such that the various increments are given by

$$\Delta\underset{\sim}{S}_{ep}(\underset{\sim}{Y}^i_{\ell+1}) = [D_{ep}(\underset{\sim}{Y}^i_{\ell+1})]\Delta\underset{\sim}{L}(\underset{\sim}{Y}^i_{\ell+1}) \tag{3.46}$$

$$\Delta\underset{\sim}{L}(\underset{\sim}{Y}^i_{\ell+1}) = [B_U^*(\underset{\sim}{Y}^i_{\ell+1})](\underset{\sim}{Y}^i_{\ell+1} - \underset{\sim}{Y}^o_{\ell+1}) \tag{3.47}$$

$$\Delta\underset{\sim}{S}_{epC}(t_{k-1}^\lambda + \lambda_k^{\nabla}\Delta t) = -[D_{ep}(\underset{\sim}{Y}_k)]\Delta\underset{\sim}{L}_C(t_{k-1}^\lambda, \lambda_k^{\nabla}\Delta t) \tag{3.48}$$

$$\Delta \underset{\sim}{S}_{ept}(t_{k-1}^{\lambda} + \lambda_k^{\nabla}\Delta t) = - [D_{ep}(\underset{\sim}{Y}_k)]\alpha(T(t_\ell^\lambda))(T(t_\ell^\lambda+\lambda_k^{\nabla}\Delta t) - T(t_\ell^\lambda)) \quad (3.49)$$

$$\Delta \underset{\sim}{S}^i_{epC}(t_\ell^\lambda+\Delta t) = - [D_{ep}(\underset{\sim}{Y}^i_{\ell+1})]\Delta \underset{\sim}{L}_C(t_\ell^\lambda,\Delta t) \quad (3.50)$$

$$\Delta \underset{\sim}{S}^i_{ept}(t_\ell^\lambda+\Delta t_{\ell+1}) = - [D_{ep}(\underset{\sim}{Y}^i_{\ell+1})]\alpha(T(t_\ell^\lambda))(T(t_\ell^\lambda+\Delta t) - T(t_\ell^\lambda)) \quad (3.51)$$

To check the convergence of the foregoing algorithm, several tests are employed. These include:

i) Definiteness check:

$$(\alpha_{2I})^2 - \alpha_{1I}\alpha_{3I} > 0 \quad (3.52)$$

ii) Pseudo force norm check:

$$\frac{||\underset{\sim}{F}(t_\ell^\lambda+\lambda_{\ell+1}^{i+1}\Delta t) - \underset{\sim}{F}(t_\ell^\lambda+\lambda_{\ell+1}^{i}\Delta t)||}{||\underset{\sim}{F}(t_\ell^\lambda+\lambda_{\ell+1}^{i+1}\Delta t)||} < \varepsilon_F \quad (3.53)$$

iii) Displacement norm check:

$$\frac{||\underset{\sim}{Y}^{i+1}_{\ell+1} - \underset{\sim}{Y}^{i}_{\ell+1}||}{||\underset{\sim}{Y}^{i+1}_{\ell+1}||} < \varepsilon_Y \quad (3.54)$$

iv) Constraint check:

$$\frac{\lambda_{\ell+1}^{i+1} - \lambda_{\ell+1}^{i}}{\lambda_{\ell+1}^{i+1}} < \varepsilon_\lambda \quad (3.55)$$

The preceeding tests are applied at different phases of the iteration process. Test i) is used to resize the HECS by self-adaptively readjusting μ_A the aspect ratio so as to guarantee an intersection with the INR extrapolation and thus ensure a convergent solution [6]. Test ii) is employed to monitor the monotonicity of successive load excursions. Lastly tests iii) and iv) are used to quantify when adequate convergence has been achieved.

Once convergence is obtained for a given time step, the overall solution algorithm must be prepared for the next interval. This requires that the various field variables are properly updated. Specifically this includes such terms as $\underset{\sim}{Y}$, $\underset{\sim}{S}_{ep}$, $\underset{\sim}{S}_{epC}$, $\underset{\sim}{S}_{epT}$ and t. In this context, if we let $I_{\ell+1}$ designate the number of iterations required to yield convergence of the $(\ell+1)^{th}$ time step, then $\underset{\sim}{Y}$ at the outset of the $(\ell+2)^{th}$ is given by the expression

$$\underset{\sim}{Y}^0_{\ell+2} = \underset{\sim}{Y}^0_{\ell+1} + \sum_{k=1}^{I_{\ell+1}} \Delta \underset{\sim}{Y}^k_{\ell+1} \quad (3.56)$$

Note as the iteration process converges, the constraints $\lambda^{i}_{\ell+1}$ represent a sequence which approaches the limit (cluster) point $\lambda^{\nabla}_{\ell+1}$ namely

$$\lambda^{1}_{\ell+1},\ \lambda^{2}_{\ell+1},\ \lambda^{3}_{\ell+1},\ldots,\ \lambda^{i}_{\ell+1},\ldots,\ \lambda^{\nabla}_{\ell+1} \tag{3.57}$$

In this context, the time at the start of the $(\ell+1)^{th}$ step is given by

$$t^{\lambda}_{\ell+1} = t^{\lambda}_{\ell} + \lambda^{\nabla}_{\ell+1}\,\Delta t \tag{3.58}$$

Now, based on (3.56) and (3.58), it follows that the various stress partitions take the form

$$\underset{\sim}{S}_{ep}(\underset{\sim}{Y}^{o}_{\ell+2}) = \underset{\sim}{S}_{ep}(\underset{\sim}{Y}^{o}_{\ell+1}) + \Delta\underset{\sim}{S}_{ep}(\underset{\sim}{Y}^{o}_{\ell+2}) \tag{3.59}$$

$$\underset{\sim}{S}^{o}_{epC}\Big|_{t^{\lambda}_{\ell+1}+\Delta t} = \underset{\sim}{S}_{epC}(t^{\lambda}_{\ell+1}) + \Delta\underset{\sim}{S}^{o}_{epC}(t^{\lambda}_{\ell+1}+\Delta t) \tag{3.60}$$

$$\underset{\sim}{S}^{o}_{epT}\Big|_{t^{\lambda}_{\ell+1}+\Delta t} = \underset{\sim}{S}_{epT}(t^{\lambda}_{\ell+1}) + \Delta\underset{\sim}{S}^{o}_{epT}(t^{\lambda}_{\ell+1}+\Delta t) \tag{3.61}$$

such that the various increments are defined by the expressions:

$$\Delta\underset{\sim}{S}_{ep}(\underset{\sim}{Y}^{o}_{\ell+2}) = [D_{ep}(\underset{\sim}{Y}^{o}_{\ell+2})]\Delta\underset{\sim}{L}(t^{\lambda}_{\ell+1}) \tag{3.62}$$

$$\Delta\underset{\sim}{L}(t^{\lambda}_{\ell+1}) = [B^{*}_{U}(\underset{\sim}{Y}^{o}_{\ell+2})](\underset{\sim}{Y}^{o}_{\ell+2} - \underset{\sim}{Y}^{o}_{\ell+1}) \tag{3.63}$$

$$\underset{\sim}{S}_{epC}(t^{\lambda}_{\ell+1}) = \sum_{k=1}^{\ell+1} \Delta\underset{\sim}{S}_{epC}(t^{\lambda}_{k-1} + \lambda^{\nabla}_{k}\Delta t) \tag{3.64}$$

$$\underset{\sim}{S}_{epT}(t^{\lambda}_{\ell+1}) = \sum_{k=1}^{\ell+1} \Delta\underset{\sim}{S}_{epT}(t^{\lambda}_{k-1} + \lambda^{\nabla}_{k}\Delta t) \tag{3.65}$$

$$\Delta\underset{\sim}{S}^{o}_{epC}(t^{\lambda}_{\ell+1} + \Delta t) = -[D_{ep}(\underset{\sim}{Y}^{o}_{\ell+2})]\Delta\underset{\sim}{L}_{C}(t^{\lambda}_{\ell+1},\ \Delta t) \tag{3.66}$$

$$\Delta\underset{\sim}{S}^{o}_{epT}(t^{\lambda}_{\ell+1} + \Delta t) = -[D_{ep}(\underset{\sim}{Y}^{o}_{\ell+2})]\alpha(T(t^{\lambda}_{\ell+1}))(T(t^{\lambda}_{\ell+1} + \Delta t) - T(t^{\lambda}_{\ell+1})) \tag{3.67}$$

Note for the present purposes, to enhance the speed of calculation of the stiffness inverse, the BFGS [3,7] scheme is employed. This approach was chosen over the straight updating scheme which is particularly expensive when several iterations are involved. Such situations typically occur in the vicinity of buckling points.

As was noted earlier, if the INR type scheme is employed to solve the thermomechanical problem, uniform time stepping in the thermal phase of calculations also leads to equal time intervals for the mechanical stage. In contrast, the use of constraints in the INR methodology yields

unequal time stepping requirements for the mechanical phase. Namely, the following type thermomechanical history is obtained, that is

t	$T(t)$	$\underset{\sim}{S}(t)$	...
0	$T(0)$	$\underset{\sim}{S}(0)$	...
$\lambda_1^{\nabla}\Delta t$	$T(\lambda_1^{\nabla}\Delta t)$	$\underset{\sim}{S}(\lambda_1^{\nabla}\Delta t)$	...
$t_1^{\lambda} + \lambda_2^{\nabla}\Delta t$	$T(t_1^{\lambda} + \lambda_2^{\nabla}\Delta t)$	$\underset{\sim}{S}(t_1^{\lambda} + \lambda_2^{\nabla}\Delta t)$	...
$\vdots$	$\vdots$	$\vdots$	
$t_\ell^{\lambda} + \lambda_{\ell+1}^{\nabla}\Delta t$	$T(t_\ell^{\lambda} + \lambda_{\ell+1}^{\nabla}\Delta t)$	$\underset{\sim}{S}(t_\ell^{\lambda} + \lambda_{\ell+1}^{\nabla}\Delta t)$	...

where here the sequence $0, \lambda, {}^{\nabla}\Delta t, \ldots t_\ell^{\lambda} + \lambda_{\ell+1}^{\nabla}\Delta t$ is typically nonuniform. Because of this, the temperature data required to generate the thermal strains and material properties are interpolated from the uniformly generated data.

BENCHMARKING

In the preceeding sections, a specialized HECS constrained BFGS updated INR time stepping strategy has been developed. The methodology enables the static solution of pre and postbuckling thermomechanical problems. In order to thoroughly evaluate the procedure, several highly nonlinear benchmark problems were undertaken. The main thrust of this work was to ascertain the capability of the constraint methodology to deal with thermomechanical problems involving:

a) Large deformation kinematics including the possibility of pre and postbuckling behavior;
b) Thermoelastic-plastic-creep material behavior;
c) Temperature dependent thermomechanical material properties; as well as,
d) Time dependent thermomechanical loads with varying combinations/ interactions between the thermal and mechanical components.

This was achieved by programming the solution scheme into ADINA [9] and its complementing thermal code ADINAT [10]. Such an approach enabled benchmarking over a wide variety of geometric configurations, material types and boundary conditions. For the present purposes, the demonstrational benchmarking consists of calculating the pre and postbuckling response of an arch to various types of thermomechanical loading fields.

For demonstration purposes, Fig. 2 illustrates the geometry of the centrally loaded arch used for the benchmarking. The creep law employed is given by the expression

$$\varepsilon_c = A_0 \sigma^{A_1} t^{A_2}$$

As seen from Fig. 2, eight noded plane stress isoparametric elements are used to generate the FE simulation.

To demonstrate the numerical efficiency and stability of the improved constrained MINR time stepping scheme, the thermoelastic-plastic-creep pre-postbuckling problem depicted in Fig. 3 is considered. As can be seen from this figure, the problem is driven into the postbuckling range of behavior by the time dependent growth of creep. Overall, the creep generated reshaping initiates a redistribution in the internal loads hence causing a change in load carrying capacity. Due to the nature of redistribution, plasticity is initiated in the later stages of postbuckling. Noting Fig. 3, $t_{critical}$ marks the time at which the pre to postbuckling transition occurs. This time zone is marked by changes in the definiteness of the structural stiffness. Table 1 illustrates the numerical efficiency/stability of the BFGS updated constrained scheme in capturing such behavior. In the case of Δt = .8 hours, Table 1, the improved algorithm yielded 210% reduction in computer time over the constrained MINR scheme. Note the classical unconstrained INR scheme completely fails in such zones of behavior for any choice of Δt. As the time step is increased further, unless some intermediate updating is employed, even the constrained MINR approach fails. This is in contrast to the BFGS updated scheme which shows significantly enhanced convergence, efficiency and stability characteristics.

As a more severe test of the scheme, we shall consider the case of cyclical creep loading problems wherein buckling occurs after several cycles. Figure 4 illustrates the load deflection behavior of the arch under a cyclically applied external load. As can be seen, as the load is cycled the accumulated creep over the various cycles progressively reduces the buckling limit of the arch. In essence, after several cycles the arch behaves as a structure with shape imperfections. Such reductions in load carrying capacity are illustrated in Fig. 5. Specifically, this figure depicts successive families of load-deflection curves which illustrate the decrease of buckling strength with time. Note, due to the efficiency and stability of the improved constrained MINR time stepping scheme, problems involving variable/cyclic loading environments can be handled more effectively.

The last example considered consists of the thermally induced buckling of the bimetallic arch depicted in Fig. 6. Noting Fig. 7, as the arches temperature is raised, a critical value is reached wherein excessive deflections occur with no essential raise in T. Such behavior constitutes the thermal equivalent of buckling. This follows from the fact that the structural stiffness is indefinite during the event.

SUMMARY

As noted earlier, the main thrust of this work has been to develop an improved solution procedure for elastic-plastic creep pre-postbuckling problems. Also of major importance is the maintenance of maximum algorithmic compatibility with currently available general purpose codes such as ADINA, ANSYS, MARC, NASTRAN, etc. As can be seen from the proceeding benchmarking, the improved constrained scheme developed herein significantly enhances the numerical operating characteristics of MINR type algorithms. It should be further noted that due to the manner of formulation, the overall procedure can be encoded into most general purpose codes with little rearchitecturing of the programming.

ACKNOWLEDGEMENT

The first author is grateful to Dr. C. Chamis of NASA-Lewis for the stimulating discussions and encouragements during the course of this work.

REFERENCES

1. Bathe, K.J.: FINITE ELEMENT PROCEDURES IN ENGINEERING ANALYSIS. Prentice Hall Inc., Englewood Cliffs, New Jersey, 1982.

2. Padovan, J.: Self Adaptive Incremental Newton-Raphson Algorithms. Symposium on Computer Methods in Nonlinear Structures and Solid Mechanics, Washington D.C., also NASACP-2147, 1980.

3. Bathe, K. J. and Cimento, A. P.: Some Practical Problems for the Solution of Nonlinear Finite Element Equations. Comp. Meth. Appl. Mech. Engrg., 22, 59, 1980.

4. Riks, E.: An Incremental Approach to the Solution of Snapping and Buckling Problems. Int. J. Solids Structures, 15, 529 (1979).

5. Crisfield, M. A.: A Fast Incremental/Iterative Procedure that Handles Snapthrough. Computers and Structures, 13, 55-62 (1981).

6. Padovan, J. and Arechaga, T.: Formal Convergence Characteristics of Elliptically Constrained Incremental Newton-Raphson Algorithms. Int. J. Engrg. Sci., 20, 1077, 1982.

7. Padovan, J., Tovichakchaikul, S., Arechaga, T.: Operating Characteristics of Hyperbolically and Elliptically Constrained Self-Adaptive Incremental Newton-Raphson Algorithms. Jr. Franklin Inst.

8. Mendelson, A.: PLASTICITY: THEORY AND APPLICATION. MacMillan, New York, 1968.

9. Bathe, K. C.: ADINA: A Finite Element Program for Automatic Dynamic Incremental Nonlinear Analysis. Rept. No. 8244-1, MIT, Cambridge, MA, 1978.

10. Bathe, K. C.: ADINAT: A Finite Program for Automatic Dynamic Incremental Nonlinear Analysis of Temperatures. MIT, Cambridge, MA, Rept. No. 82448-5, 1978.

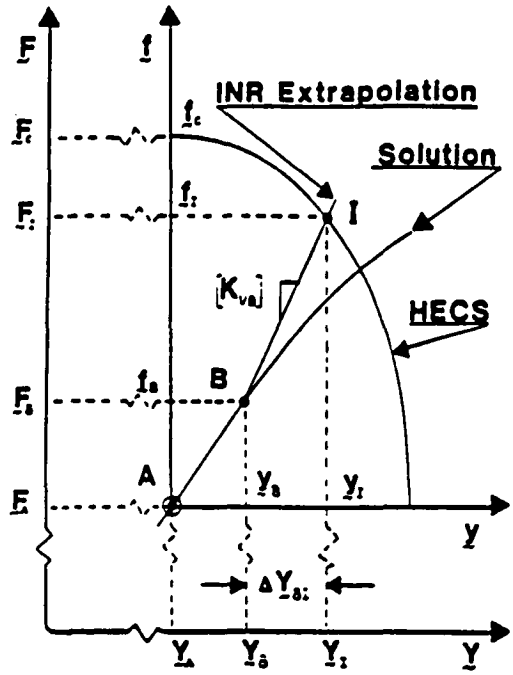

Fig.1 HECS constrained INR iterations

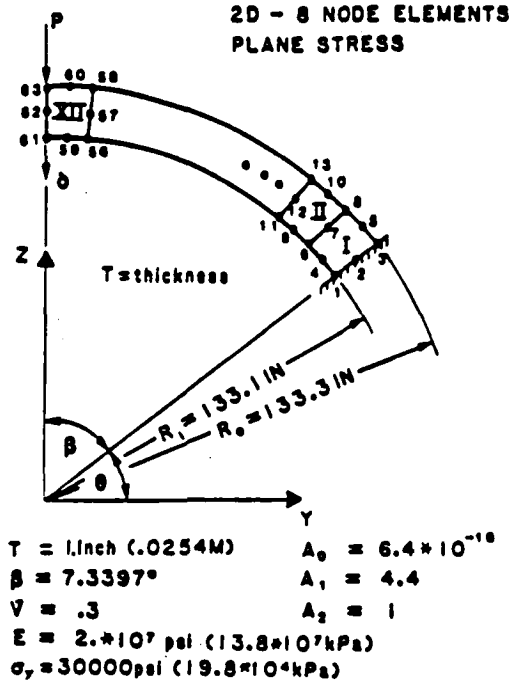

Fig.2 Centrally loaded arch

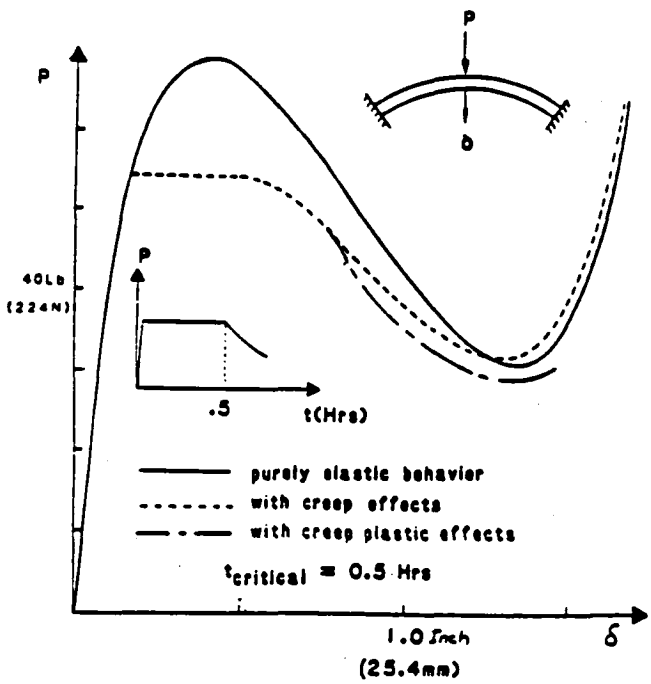

Fig.3 Single cycle arch response

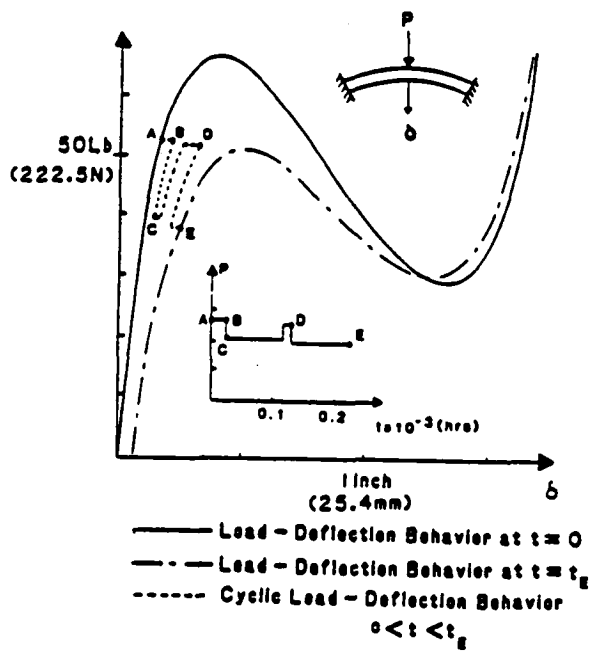

Fig.4 Multi-cycle arch response

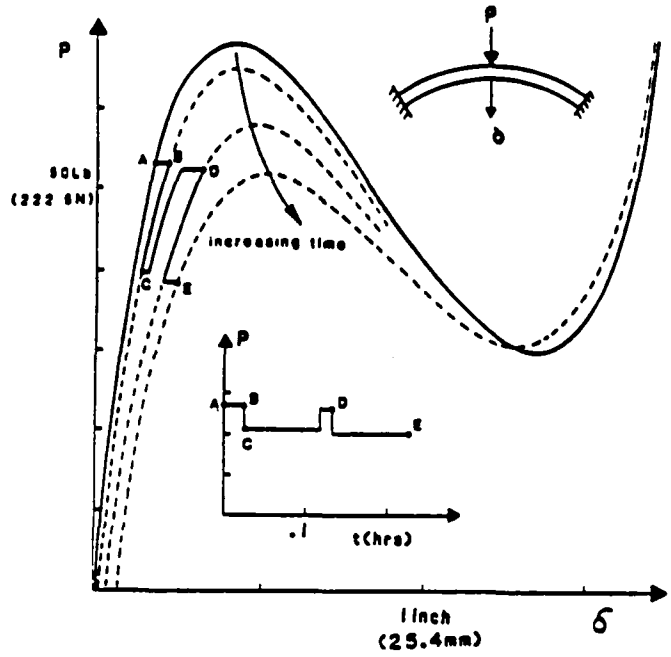

Fig.5 Cyclical degradation of arch stability

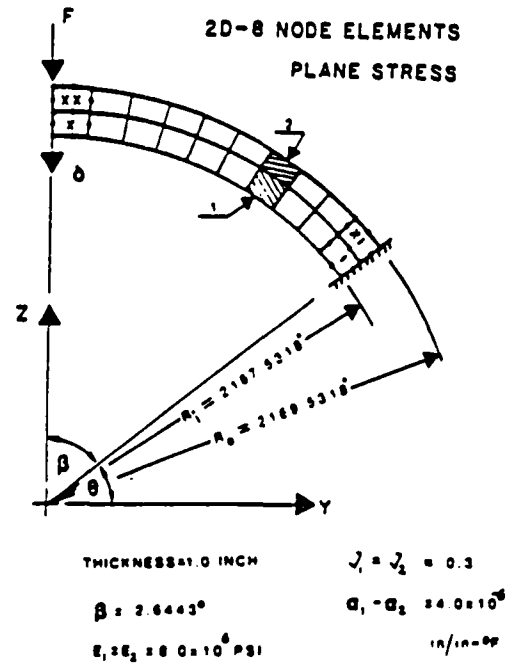

Fig.6 Bimetallic arch

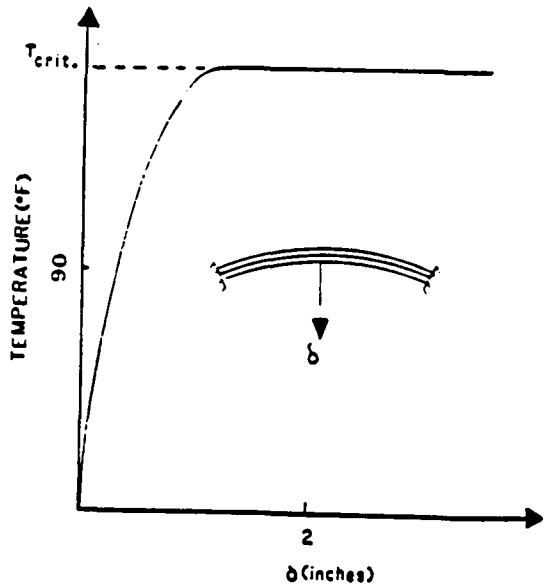

Fig.7 Response of bimetallic arch to uniform temperature

Step	No. of Iteration Δt = .8 Hrs.		
	Classical MINR	Constrained MINR	Improved Constrained MINR
1-17	SOLUTION FAILED OUT OF BALANCE LOADS	.	.
18		3	3
19		4	3
20		5	4
21		7	4
22		12	5
23		32	5
24		40	5
25		9	4
26		4	3
27		3	3
28		3	2
29		2	1
30		1	1
		.	.
		.	.
		.	.

Table 1 Numerical comparisons